

1

AD-A212 553

An Efficient Enhancement of
Finite-Difference Implementations
for Solving Parabolic Equations

by

J. S. Robertson, M. J. Jacobson,
W. L. Siegmann, and D. C. Arney

DTIC
ELECTE
SEP 19 1989
D D

Department of Mathematical Sciences

Rensselaer Polytechnic Institute

Troy, NY 12180-3590

RPI Math. Rep. No. 177

September 15, 1989

This work is sponsored by

Code 1125 OA, Office of Naval Research

Contract No. N00014-86-K-0129

NR 4254007

This document has been approved for public release and sale; its distribution
is unlimited.

89 9 18 138

An efficient enhancement of finite-difference implementations for solving parabolic equations

J. S. Robertson and D. C. Arney

Department of Mathematics, United States Military Academy, West Point, New York 10996-1786

M. J. Jacobson and W. L. Siegmann

Department of Mathematical Sciences, Rensselaer Polytechnic Institute, Troy, New York 12180-3590

(Received 9 October 1988; accepted for publication 17 March 1989)

The parabolic approximation method is widely recognized as useful for accurately analyzing and predicting sound transmission intensity in diverse ocean environments. One reason for its attractiveness is that solutions are marched in range, thereby avoiding the large internal storage requirements when using the full wave equation. Present finite-difference implementations employ a range step size that is prescribed by either the user or the code and that remains fixed for the duration of the computation. An algorithm is presented in which the range step is adaptively selected by a procedure within a version of the implicit finite-difference (IFD) implementation of the parabolic approximation. An error indicator is computed at each range step, and its value is compared to an error tolerance window that is readily specified by the user. If the error indicator falls outside this window, a new range step size is computed and used until the error indicator again leaves the tolerance window. Furthermore, for a given tolerance, this algorithm generates a range step size that is optimal in a specified sense and that often leads to large decreases in run time. Additional related modifications to the IFD implementations are discussed. Several examples are presented that illustrate the efficacy of the enhanced algorithm.

PACS numbers: 43.30.Bp

(KR) ←

A-1 20

For	
A&I	<input checked="" type="checkbox"/>
3	<input type="checkbox"/>
ed	<input type="checkbox"/>
ility Codes	
il and/or	
Special	

INTRODUCTION

Since its introduction to the underwater acoustics community more than a decade ago,¹ the parabolic approximation to the reduced wave equation has seen widespread application in many important underwater sound propagation problems. This type of approximation easily and accurately handles strongly range-dependent environments, offering a capability beyond the reach of normal mode theory and related methods. Since it is effective at low frequencies, it is suitable for analyzing and predicting propagation in situations where diffraction may be important, thus offering a significant advantage over ray theory. Another reason for interest in this method is computational efficiency. The fruits of this approximation are parabolic equations (PEs) that can be marched in range, thereby saving considerable amounts of internal core storage.

Numerical implementations of PEs have been developed using different algorithms. One of these, using an implicit finite-difference scheme,² is well suited to ocean environments in which there are significant amounts of acoustic interaction with the ocean bottom. Other algorithms, based on the split-step method³ (which uses fast Fourier transforms), have proven advantageous for modeling deep-ocean sound channel propagation. Both types of algorithms have been refined in many ways. For example, the implicit finite-difference algorithm has been extended to handle wide-angle PEs,⁴ while the split-step method has been implemented on a high-speed, special-purpose array processor.⁵

Although PEs offer significant computational advantages over methods for the (elliptic) Helmholtz equation, many propagation problems pose formidable computational

problems and may be infeasible with present codes. For example, results in the time domain can be obtained by solving a PE for many different frequencies in the same channel and then superposing the results with Fourier transforms.⁶ Broadband problems solved by this method require dozens, perhaps hundreds, of computations at different frequencies. Also, high-frequency propagation problems may require computational meshes of prohibitively small size, making solutions simply too expensive to compute. Deep-ocean channels of long range can require large amounts of time, limiting the ability to perform simulated propagation studies under a variety of interesting conditions. In addition, certain classes of three-dimensional problems can be computed by two-dimensional solutions through vertical slices of the ocean.⁷ For sufficiently large azimuthal regions, this method clearly requires large amounts of time for each computation.

There is a clear and pressing need for substantially faster propagation codes.⁸ In part, this requirement for speed will be satisfied with more powerful computers, such as array processors and supercomputers,⁹ which may become available in a few years. Even so, computational acoustic algorithms must be made as efficient as possible, regardless of the type of machine. One way to significantly contribute toward the goal of obtaining optimal efficiency is through the use of adaptive computational methods. In these, the mesh consisting of the set of discrete points at which the solution is computed is adjusted so that the number of points used is minimized while some measure of the solution accuracy is preserved. For example, one implementation of the split-step method³ employs adjustments of range step size based on truncation error estimates that, in turn, depend on partial derivatives of the refractive index. In addition, depth step

size can increase, but not decrease, in response to specialized conditions obtained from spectral energy estimates.

It is the purpose of this paper to describe a method for accomplishing part of this objective for finite-difference methods. We emphasize here that the approach we describe is substantially different from the one employed in Ref. 3. In addition, the focus of our work is on the performance accuracy on the adaptive algorithm as well as its efficiency. In Sec. I, a two-dimensional narrow-angle parabolic approximation and a finite-difference algorithm implementation for solving the resulting PEs are reviewed. Notation pertinent to the discretized PE solution, as well as a discussion of current methods of selecting fixed mesh sizes, are presented. An error indicator is introduced and a method for adaptively selecting the range step using this indicator is discussed in Sec. II. In Sec. III are presented several examples that demonstrate the computational advantages attained by adaptively selecting the range step. Finally, Sec. IV contains a summary of our principal results.

I. THE PARABOLIC APPROXIMATION AND IFD IMPLEMENTATION

Parabolic approximations typically begin from the Helmholtz equation

$$\nabla^2 p + k_0^2 n^2 p = 0, \quad (1)$$

which governs the acoustic pressure field p in a steady, quiescent medium due to a harmonic point source of frequency f . In Eq. (1), $k_0 = 2\pi f/c_0$ is the wavenumber, $n = c_0/c(r, \theta, z)$ is the index of refraction, $c(r, \theta, z)$ is the sound speed, and c_0 is a reference sound speed. The farfield assumption is given by

$$p = u(r, \theta, z) H_0^{(1)}(k_0 r), \quad (2)$$

where $H_0^{(1)}(k_0 r)$ is the Hankel function of the first kind of order zero. Equation (2), assumed to hold for sufficiently large values of r , supposes that there are only outward traveling waves, i.e., no backscattering. The quantity $u(r, \theta, z)$ is a slowly varying function of position that modulates the Hankel function. If Eq. (2) is substituted into Eq. (1), and appropriate conditions are satisfied, the following "standard PE" can be shown to hold:

$$2ik_0 u_r + u_{zz} + k_0^2 (n^2 - 1)u = 0. \quad (3)$$

Since no θ derivatives appear in Eq. (3), we suppress the θ dependence of u and write $u(r, z)$. Details on the derivation of Eq. (3) can be found in Refs. 1, 10, and elsewhere. It is important to note that Eq. (3) is not the only parabolic approximation that could be derived. Other examples include PEs for three-dimensional propagation¹¹ and wide-angle propagation,¹² and additional ones can be obtained from more general versions of Eq. (1). For example, PEs have been derived that are appropriate for sound channels in which the medium is moving¹⁰ or the density is variable.

There are several numerical algorithms available for solving Eq. (3), together with an appropriate set of boundary and initial conditions. In particular, one using implicit finite differencing of the partial derivatives has been widely distributed in the underwater acoustics community. Details of this finite-difference algorithm can be found in Ref. 13. It utilizes a Crank-Nicolson scheme to march the solution in

range with a formal order of accuracy of $O[(\Delta r)^2 + \Delta(z^2)]$, where Δr and Δz are the range and depth step sizes, respectively. This method is popular for parabolic systems because of its accuracy and absolute stability. One advantage to this approach is its particularly convenient ability to model horizontal as well as irregular interfaces between layers with different acoustic properties. The implementation, known as implicit finite-difference (IFD) implementation, contains a number of powerful and flexible features that permit its application to a broad variety of ocean acoustic environments. For instance, an input stream provides a mechanism for the user to prescribe source data, specify selected numerical parameters such as mesh size, describe many types of complex propagation environments, and select a variety of output options. IFD implements pressure-release and rigid boundary conditions on flat or sloping boundaries, and matches the wave field from the water column into any number of sub-bottom layers with different densities, sound speeds, and volume attenuations. It also contains a feature to apply an artificial absorbing layer (beneath sub-bottom layers) that is used to enforce a pressure-release bottom boundary in many applications. The code generates several output files, including ones containing the complex-valued solution to the PE, as well as the transmission loss. Additional features are available and are documented in Refs. 2 and 13. For the rest of this paper, IFD will refer to the implicit finite-difference implementation described in Ref. 2 (and modified by us for increased speed and accuracy), while EIFD will refer to the implementation including the enhancements discussed herein.

In the IFD implementation, the numerical solution of Eq. (3) is represented as u_m^n , where

$$u_m^n = u(r_m, z_n), \quad m = 1, \dots, M, \quad n = 1, \dots, N. \quad (4)$$

In Eq. (4), (r_m, z_n) corresponds to a point on the range-depth mesh, and M and N are integers indicating the maximum number of range and depth points on the mesh. Although the algorithm treats nonhorizontal boundaries by adding or deleting depth mesh points, we take N fixed throughout this paper. We note that this version of IFD only handles horizontal interfaces, so that sloping or irregular interfaces are approximated by stepwise horizontal interfaces.

IFD requires users to either specify the characteristic dimensions of the computational grid upon which the solution is computed or to accept default values. With IFD, Δr and Δz represent fixed range and depth increments, so that $r_m = m\Delta r$ and $z_n = n\Delta z$. It is not always clear *a priori* whether there are optimal choices for Δr and Δz dimensioned to minimize computation time while preserving appropriate measures of solution accuracy. In the standard IFD implementation, the typical default values are $\Delta r = \lambda/2$ and $\Delta z = \lambda/4$, where λ is the acoustic wavelength of the source signal. In general, these mesh sizes tend to be unnecessarily small. Normally, this can only be corrected when the user has had experience with computational results for a particular problem.

The geometry of the sound channel, together with values of all important parameters, is provided to IFD via an

input runstream file. Our implementation adds two additional parameters to this runstream: an error tolerance ϵ and a "cut-in" range value. These parameters will be discussed in detail in Sec. II. For output, IFD generates files containing the complex valued solution $u(r_m, z_n)$ and the transmission loss. Our implementation appends three additional files that contain the step size used at each range, an indicator of the error committed at each range step, and the cumulative range values for the transmission loss file.

II. ENHANCED IMPLEMENTATION (EIFD)

Later in this paper, we will vary the range step so that $(\Delta r)_m = r_m - r_{m-1}$ refers to the m th range step taken in the calculation. In fact, for different problems, the behavior of $(\Delta r)_m$ can actually vary in interesting ways, but often $(\Delta r)_m$ can be surprising larger than a wavelength. Consequently, significant computational advantages are obtained. Since we intend to select the range step size to control a measure of the error, we first require a method for estimating the error associated with a given step size. One such choice is

$$E(r_m) = (\Delta r)_m^2 \|\partial_{rr} u_n^m\|_2, \quad (5)$$

which indicates local error estimate and feedback to adjust the range step size. To estimate $\partial_{rr} u_n^m$ pointwise by Eq. (5) at each depth node $n = 1, \dots, N$, we use backward differences on the two previous range steps; i.e.,

$$\partial_{rr} u_n^m = \left(\frac{u_n^{m-2} - u_n^{m-1}}{(\Delta r)_{m-1}} - \frac{u_n^{m-1} - u_n^m}{(\Delta r)_m} \right) / (\Delta r)_m. \quad (6)$$

The norm used in Eq. (5) is the discrete approximation to the L_2 norm, given by

$$\|\partial_{rr} u_n^m\|_2 = \sqrt{\sum_{i=1}^N \frac{\partial_{rr} u_i^m \overline{\partial_{rr} u_i^m}}{N}}, \quad (7)$$

where the overbar denotes complex conjugation. We examined other norms, L_1 or L_∞ , but found no particular reason to select one over another, so that L_2 was chosen as a matter of convenience. For the PE, the measure given by Eq. (5) is only proportional to the true error, but is nonetheless a good error indicator. A more accurate error estimation technique, such as Richardson extrapolation, could also be implemented at the expense of additional computational overhead.^{14,15} Furthermore, this error indicator does not contain any estimate of the error caused by the discretization of the depth into steps of size Δz .

Our technique contrasts with the work of Ref. 16, which does not deal with step-changing algorithms, but which uses a measure of the local error to verify the solution accuracy after the computation of the entire solution. Furthermore, we emphasize that our error indicator is obtained directly from the computed solution, a substantially different approach from the one used in Ref. 3, which estimates truncation error of the solution in terms of certain partial derivatives of the refractive index. This latter method of error estimation is feasible for calculations performed in the wave-number domain.

We seek to control the magnitude of the error indicator Eq (5) in two ways. First, the error indicator E should be kept below a user-specified error tolerance ϵ in order to

maintain the solution accuracy. Second, E should not fall below some percentage, chosen as 70, of ϵ so that reasonable computational efficiency is achieved. When these conditions hold, the computation continues with the same value of $(\Delta r)_m$. Otherwise, if $E > \epsilon$ or $E < 0.7\epsilon$, the error indicator is controlled by adjusting the step size $(\Delta r)_m$. Our technique is similar to the step size selection used by one-step codes for ordinary differential equations described in Ref. 17. Since we are using an implicit scheme, a system of equations, whose matrix representation is tridiagonal, is solved at each range step. This calculation is efficient because of the special structure of the matrix. Since elements in this system are dependent on $(\Delta r)_m$, it is desirable to avoid modifications of $(\Delta r)_m$ at every step and the costly recomputation of matrix elements. We have found that a proper trade-off occurs with the indicator inside a tolerance window of from 70% to 100% of the error tolerance.

After any solution step, the next range step $(\Delta r)_{m+1}$ is determined from E , ϵ and $(\Delta r)_m$. For the current step, we know from Eq. (5) that $E \propto (\Delta r)_m^2$ and, to achieve accurate and efficient computation, we want the next range step size $(\Delta r)_{m+1} \propto \epsilon^{1/2}$. The following proportionality results:

$$\epsilon/E(r_m) \propto (\Delta r)_{m+1}^2 / (\Delta r)_m^2. \quad (8)$$

Consequently, if a range step adjustment is judged necessary, the new step size is determined by

$$(\Delta r)_{m+1} = \beta [\epsilon/E(r_m)]^{1/2} (\Delta r)_m, \quad (9)$$

where β is a constant of proportionality.

The parameter β provides a useful degree of freedom in our method. If the current step's error estimate is over the window ($E > \epsilon$), the adjustment is made with $\beta = \sqrt{0.7}$ in order to project the error estimate for the next step toward the bottom of the window. If the error estimate has decreased below the window ($E < 0.7\epsilon$), the choice $\beta = 1$ adjusts the next step size to an error estimation near the top of the window. These selections of β provide for maximum possible use of the window before the next range step adjustment needs to be made. We emphasize the novelty of our approach by pointing out that selection of parameters analogous to β are usually *ad hoc*.¹⁷ In contrast, we have provided herein a definite and consistent way to select its value based on the performance of the error indicator.

Another type of adjustment to $(\Delta r)_{m+1}$ may also be required to ensure that the algorithm performs adequately at vertical interfaces, which may occur at certain ranges to model rapid horizontal changes in sound-speed profile, bottom structure, or channel geometry. As a result of the basic IFD implementation, it is necessary that calculation always begin exactly at a range r_{vi} of a vertical interface. With uniform step sizes, this is usually easy to arrange, but with variable range steps, particularly when $(\Delta r)_m$ is very large, it is possible for $(r_{vi} - r_m) \ll (\Delta r)_m$. In this case, $(\Delta r)_{m+1} = r_{vi} - r_m$ and the range step is forced to be much smaller than required by the error indicator. Once the computation proceeds past the vertical interface, many more step adjustments arise from this small step, introducing undesirable computational overhead. In order to provide a smooth transition of the range step size at such an interface, our algo-

rithm checks two step sizes ahead and, when a change is necessary, makes two modest step size changes instead of one more drastic change. In particular,

$$\begin{aligned} \text{if } r_m + 2(\Delta r)_{m+1} > r_v, \\ \text{then } (\Delta r)_{m+1} = \frac{1}{2}(r_v - r_m). \end{aligned} \quad (10)$$

Occasionally, the step size from Eq. (10) is too large and the indicator leaves the window. However, within two steps, the error is typically brought back under control.

EIFD includes another enhancement appropriate for acoustic intensity calculations. Any algorithm that numerically solves a PE does not compute the wave field but, rather, the slowly modulated envelope $u(r, z)$. This quantity is then used to calculate transmission loss or relative intensity. Thus, to underwater acousticians, a meaningful error tolerance would be expressed in decibels, a form of relative error, while a more natural way to control error is in terms of the absolute units in which the envelope function is computed. Clearly, near regions where the solution norm is zero or nearly so, the decibel error could be very large and, in fact, may be impossible to control. Thus any adaptive method should be constructed to locate deep fades and indicate their size to some extent, but not to accurately predict how many decibels are lost at the fade. We now describe one way to relate the absolute error ϵ to a relative error q , expressed in decibels.

Let \tilde{u} be the true solution to Eq. (3) and u the computed solution at some mesh point, with E the computed value of the error indicator. We seek an estimate for the error q in decibels. Note that

$$\left| |\tilde{u}| - |u| \right| \leq kE, \quad (11)$$

where k is a positive constant. Equation (11) is one way to state that the true error is proportional to the error indicator. This expression can be reformulated as

$$\begin{aligned} 20 \log_{10}(1 - kE/|u|) &\leq 20 \log_{10}|u| - 20 \log_{10}|\tilde{u}| \\ &\leq 20 \log_{10}(1 + kE/|u|). \end{aligned} \quad (12)$$

From Eq. (12), we get bounds on the decibel error q , specifically

$$\begin{aligned} q &= |20 \log_{10}|u| - 20 \log_{10}|\tilde{u}|| \\ &\leq 20|\log_{10}(1 - kE/|u|)|. \end{aligned} \quad (13)$$

In general, q is small since the error tolerance ϵ is typically selected to force $E \ll |u|$. However, near a null or deep fade, q could become large since E may equal or substantially exceed $|u|$. This is one reason why the transmission loss (or relative intensity), which is measured in decibels, when calculated adaptively, may exhibit substantial error in the vicinity of deep fades and other locations where the solution magnitude and error tolerance are of comparable size.

We can use Eq. (13) to generate a choice of error tolerance for a prescribed level of decibel error q , which will be valid away from deep fades. It follows from Eq. (13) and $E > 0.7\epsilon$ that

$$\epsilon \leq (10|u|/7k)(1 - 10^{-q/20}). \quad (14)$$

An optimal numerical value for k is uncertain, but from our numerous computations, it appeared that $k \approx 0.1$ in many

cases. An uncertainty of $q = 1$ dB seems to be a reasonable constraint on the size of the decibel error away from deep fades. Given these choices, a convenient selection for a value of the error tolerance, using Eq. (14), is $\epsilon = 10^{-3}$. Other choices of ϵ are discussed in Sec. III.

Before discussing specific numerical examples, we now discuss several additional features that have been included in EIFD. Often the start-up field results in many modes propagating until bottom attenuation strips the higher-order modes so that near the source, the solution looks "noisy." Within this region, the adaptive range step changer could make the range step very small. Since the nearfield is rarely of interest in calculations with EIFD, a feature has been added to the input runstream that allows the adaptive calculation to be switched on after a certain range, called the cut-in range r_o , is achieved. For example, in a particular ocean channel, it may be known that, using the usual Gaussian start-up field, the effects of bottom attenuation are largely absent until a range of 4 km. Consequently, r_o is set to this value.

It is sometimes possible that the solution to the PE is exponentially decaying. In this circumstance, the solution norm will eventually become smaller than the error tolerance, so that the error measure becomes useless. EIFD contains a feature that checks the norm of the solution vector at each step. If the norm $\|u\|_2$ is less than ten times the error tolerance ϵ , then the step size is no longer changed.

In order to monitor the progress of the adaptive calculation, several additional output files are required. Specifically, both the error indicator and the step size at each step are listed to output files. Furthermore, the value of each range at which the relative intensity is written must also be listed, so that intensity curves can be properly plotted.

III. NUMERICAL RESULTS

In order to gauge the efficacy of our algorithm, four examples will be discussed, with each example presenting a different and acoustically important environment. We have thoroughly and carefully examined the performance of our step changing algorithm, with attention focused both on solution accuracy as well as on execution time improvements. Although other, nonfinite-difference implementations have utilized range step changers, an examination, like ours, of algorithm performance is evidently novel.

All calculations were performed on a Prime 850 mini-computer. Efficiencies for each example are estimated using a performance measure that is the run-time ratio of the nonadaptive (N mode) run time to the adaptive (A mode) run time. This ratio, denoted by the symbol F , suggests the general increase in computational efficiency of the A mode when $F > 1$, but is naturally dependent to some extent on the hardware used. Nonetheless, we believe that F is both a straightforward way to measure the performance of our algorithm and a reasonable indicator of speed ratios on any system.

In each of our examples, the calculated quantity is relative intensity I , given by

$$I = 20 \log_{10} |p(r, z)| / |p_{ref}|, \quad (15)$$

where $p(r, z)$ is given by Eq. (2) and p_{ref} is a reference pres-

sure measured at $r = 1$ m from the source. Furthermore, in each example, a Gaussian starting field is used to provide an estimate of the sound field close to the source. This method is widely used because it is simple to calculate, and, in fact, is an integral part of the standard implementation of IFD. Nonetheless, other starting methods are available and could be used here as well. However, our results are not expected to depend significantly on the choice of a Gaussian starting field.

A. Isospeed horizontal channel

In this example, a cw source \mathcal{S} of frequency 200 Hz is placed at depth 25 m. The water is 100 m deep, overlying a fluid bottom that extends an additional 100 m. Finally, an artificial absorbing layer of depth 50 m is appended. Sound speed and density discontinuities appear at the interface, and the lower layer also has volume attenuation. The channel geometry, together with values of important acoustical parameters, is shown in Fig. 1. This sound channel is identical to one used in Ref. 10.

For this channel, the adaptive calculation was accomplished by selecting an error tolerance of $\epsilon = 10^{-3}$ and cut-in range of $r_c = 3$ km. The behavior of the error indicator E versus range r is shown in Fig. 2. The step size begins at $\Delta r = 5$ m, and remains constant until the cut-in range is achieved. The error indicator decreases steadily as the "noisy" start-up field is stripped by the lossy bottom. At that point, E is below the tolerance window, indicated by the pair of horizontal dashed lines. Once the step size changer is activated, Δr is increased and E is brought inside the window. The error continues to decrease, and Δr is enlarged each time E falls below the lower bound of the window. At about range $r = 36$ km, the step size is approximately 220 m, or about 26 wavelengths. That the step size could achieve such a large size and still retain accuracy of calculation may be surprising.

The accuracy of the adaptive calculation is clearly demonstrated in Fig. 3. The solid curve represents relative intensity I versus range r for a receiver depth of 25 m, using N mode with $\Delta r = 5$ m. The dashed curve is the same quantity but computed in A mode as described above. The overall shape of the intensity curve, including the location of local

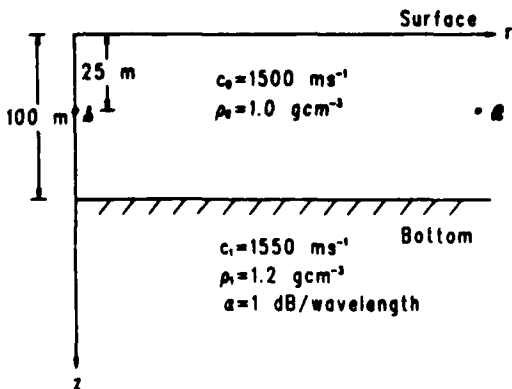


FIG. 1. Isospeed horizontal channel.

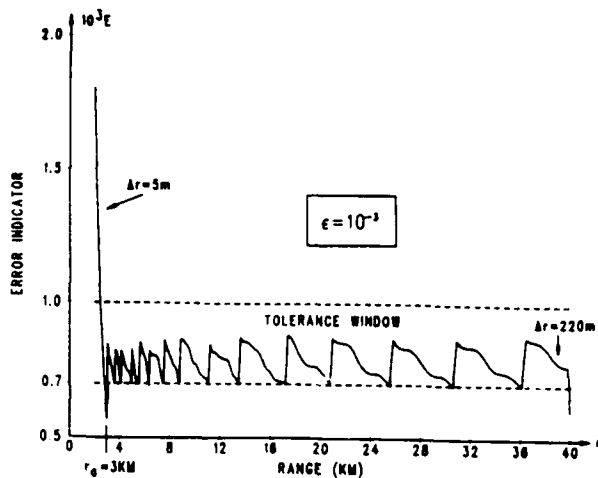


FIG. 2. Error indicator E versus range r for channel shown in Fig. 1: $f = 200$ Hz; $h_1 = 25$ m; $r_c = 3$ km; and $\epsilon = 10^{-3}$.

maxima and minima and height of the peaks, is predicted well by the adaptive calculation. The extent of deep fades can be over- or underestimated by several decibels or more. Although this is expected from our earlier discussion in Sec. II, it is of little consequence since intensity levels at deep fades are usually of little practical interest. For the example, the efficiency factor is $F = 7.3$, meaning that the adaptive calculation ran over seven times faster than the nonadaptive one.

B. Converging channel

In this example, the sound channel is range dependent. As depicted in Fig. 4, an isospeed water column with $c_0 = 1500$ m s $^{-1}$ begins at depth 350 m and lies over an interface, with a fluid layer below that possesses volume attenuation. The interface is horizontal for a range of 10 km. Then, the interface slopes upward at an angle of 8.5 deg until range 12 km, where the depth is 50 m. At that point, the interface is flat and remains so to a distance of 40 km. The lower layer always extends to depth 750 m, and an artificial

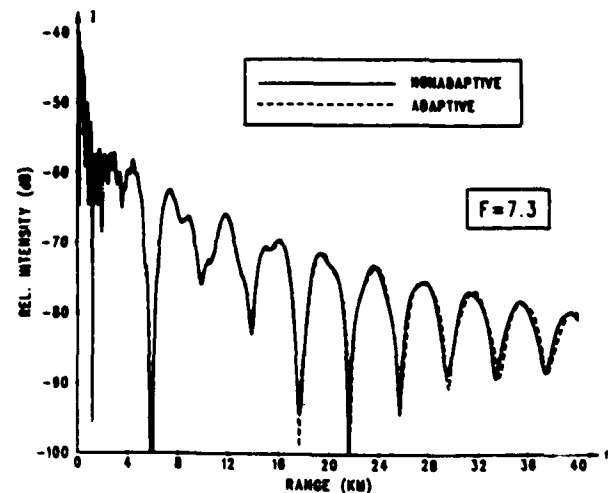


FIG. 3. Relative intensity I versus range r for parameters of Fig. 2; $h_1 = 25$ m.

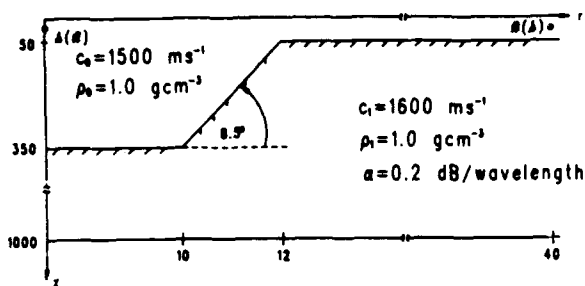


FIG. 4. Isospeed sloping channel.

absorbing layer extends an additional 250 m. This channel was described in Ref. 13. The source frequency is 25 Hz and is located at depth 25 m.

The error indicator as a function of range is depicted in Fig. 5. The step size was held fixed at $\Delta r = 10$ m until the cut-in range $r_c = 4$ km. Note that the error tolerance used in this example is $\epsilon = 1.5 \times 10^{-4}$. This value was chosen to force the tolerance and the error indicator to have approximately similar magnitudes at the cut-in range, preventing rapid and severe step size adjustments. The step size continues to increase until $\Delta r = 25$ m at the foot of the slope where $r = 10$ km. The sudden rapid change in E seen at that point is caused by step truncation at the vertical interface at the start of the slope as was discussed in Sec. II. As the sound propagates upslope, the error starts to increase steadily and is controlled by reducing step size, until $\Delta r = 9$ m at the top of the slope. Again, a step truncation occurs at $r = 12$ km for the reason just mentioned. After E is under control, the error decreases in a somewhat regular manner, permitting step size to be increased until $\Delta r = 96$ m at range near $r = 24$ km. This step size corresponds to 1.6 wavelengths. Beyond 24 km, E decreases rapidly and no more step adjustments are made. The reason is that the solution norm is too small and the algorithm has stopped changing step size. For this particular sound channel, the step size changer makes nearly full use of the tolerance window. We note that this error

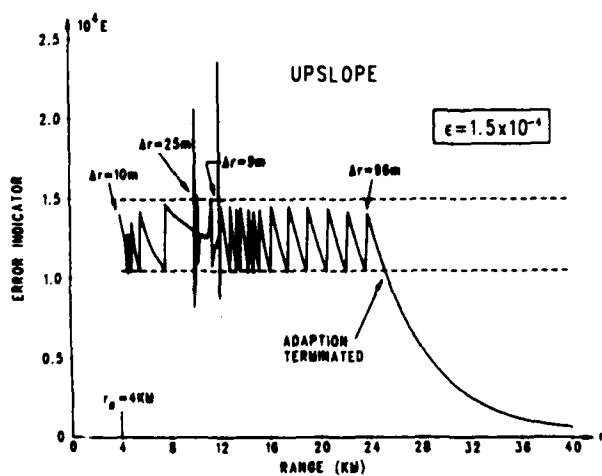


FIG. 5. Error indicator E versus range r for the isospeed sloping channel shown in Fig. 4, with source S at the left and receiver R at the right; $f = 25$ Hz; $h_s = 25$ m; $r_c = 4$ km; and $\epsilon = 1.5 \times 10^{-4}$.

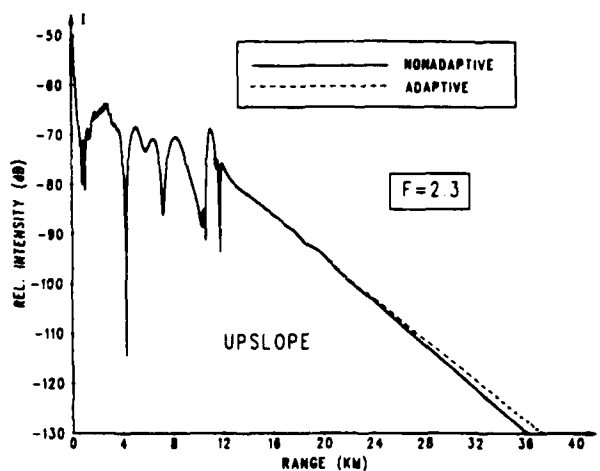


FIG. 6. Relative intensity I versus range r for parameters of Fig. 5: $h_s = 25$ m.

behavior, while desirable in every case, is not fully achieved in all sound channels (see Fig. 2).

A comparison between N mode and A mode intensities is shown in Fig. 6. As in our first case, the receiver depth is 25 m. The solid curve depicts relative intensity versus range for the N mode solution, while the dashed curve depicts I for the A mode calculation. As can be seen, acoustic mode cutoff occurs near the top of the slope. Thus the sound field decays exponentially beyond this range, accounting for why the step changer stopped. Some error is noticeable between the two intensity curves, but the agreement is extremely good. Furthermore, the efficiency factor $F = 2.3$. While not as dramatic as the isospeed problem, this result represents a substantial improvement in computation time.

C. Diverging channel

This channel is physically identical to the one just described. However, the source S and receiver R have been interchanged, so that the sound propagates to 10 km in very shallow water, travels down a steep slope, then propagates out to 40 km in water 350 m deep. Pertinent environmental

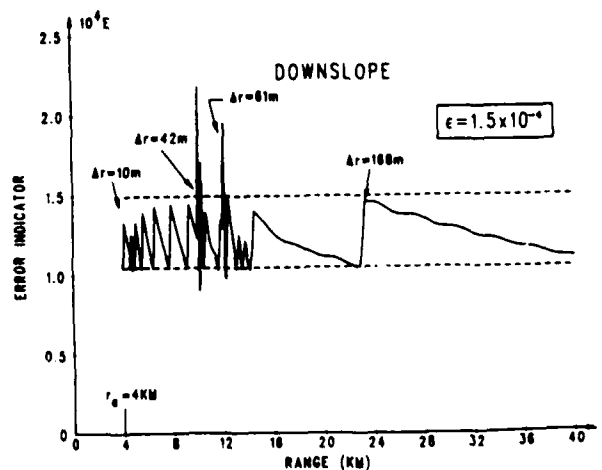


FIG. 7. Error indicator E versus range r for channel shown in Fig. 4, but with source S and receiver R interchanged; parameters as in Fig. 6.

parameters and source/receiver depths remain the same.

The behavior of the error indicator is shown in Fig. 7. Values for the error tolerance and cut-in range are the same as those used in Fig. 5. Beyond r_0 , step size is rapidly increased until $\Delta r = 42$ m at the top of the slope. After the occurrence of step truncation at that point, E decreases each time Δr is changed. Consequently, Δr is increased as the sound propagates downslope, which is the opposite behavior from what occurred when propagation was upslope. At $r = 12$ km, there is another step truncation and Δr changes increases times. Near 14 km, a marked decrease occurs in the rate of decrease of E with increasing range. In fact, the final change in step size occurs at $r = 24$ km, where $\Delta r = 168$ m, corresponding to 2.8 wavelengths. This step size is substantially larger than the terminal step used in Fig. 5.

Computed intensities are depicted in Fig. 8. The solid curve represents relative intensity I without adaption, while the dashed curve shows intensity calculated with the error tolerance and cut-in range of Fig. 7. Agreement is excellent between both calculations up through and well past the sloping region. Beyond about $r = 20$ km, there are some observable phase shifts in both peaks and fades. Nonetheless, the qualitative picture of fades and peaks intensity in the channel, along with levels at most of the peaks, is represented very well. Recall that in the previous example, adaptation was terminated at $r = 24$ km, where the relative intensity was about -100 dB. In Fig. 8, the solution norm beyond the slope is just barely above the termination criterion. Consequently, inaccuracies inevitably creep into the computation. Naturally, more accuracy can be attained with stricter values of the error tolerance ϵ . Finally, the efficiency factor is $F = 4.8$ for the two runs of Fig. 8. This figure is substantially higher than that for Fig. 6 for the same physical channel, and indicates a nearly fivefold decrease in run time for the A mode calculation.

D. Deep-ocean channel

In this example, a deep-ocean channel with moderately refracting sound-speed profile was used. This example is similar to one used in Ref. 18. The profile contains a front,

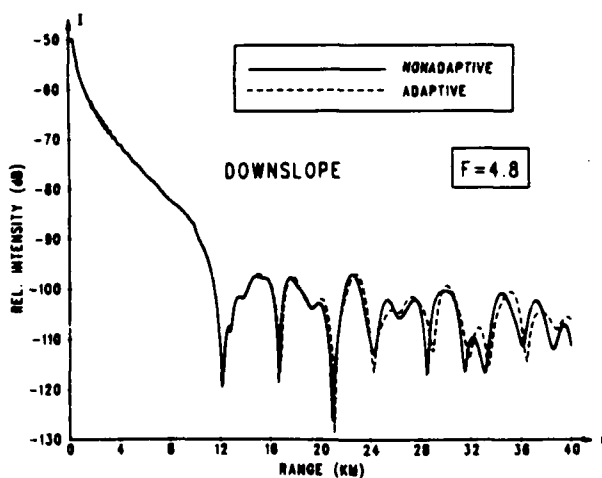


FIG. 8. Relative intensity I versus range r for parameters in Fig. 6.

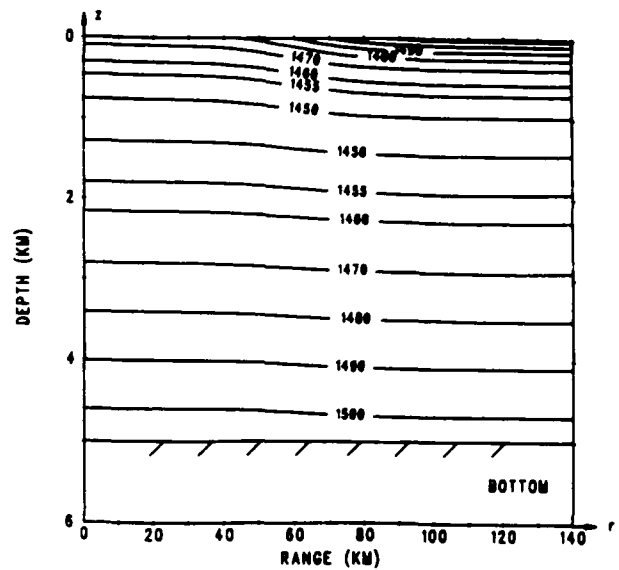


FIG. 9. Level curves of sound speed (m s^{-1}) versus range and depth (km) for a deep-water sound channel.

located at range 50 km, as suggested in Fig. 9. The sound speed is given by

$$c(r, z) = c_0 [1 + \xi(r)(e^{-\eta} + \eta - 1)], \quad (16)$$

where c_0 , $\xi(r)$, and $\eta(r, z)$ are given in Table I. This sound-speed profile is a modification of Munk's canonical deep-water profile. The channel is 5 km deep and an artificial absorbing bottom of depth 1 km is used. The source is at depth 100 m, and the source frequency is 100 Hz.

The behavior of the error indicator is shown in Fig. 10. For this calculation, the error tolerance is $\epsilon = 10^{-3}$ and cut-in occurs at $r_0 = 40$ km. The cut-in distance is large because the error indicator E decreases much more slowly than in any of the previous three examples, owing to the existence of a sound channel and a lack of volume attenuation in the bottom (the artificial absorbing layer prevents reflections from the bottom boundary but does not induce exponential decay in the solution). The initial step size is $\Delta r = 10$ m,

TABLE I. Components and parameters for the range-dependent sound-speed profile of Eq. (16).

Parameter	Value or description
c_0	sound speed at channel axis, 1450 m s^{-1}
$\xi(r)$	$B(r)g/c_0$
$B(r)$	thickness of thermocline front, $B_1 + [(B_2 - B_1)/2] \tanh\{(r - r_f)/L\}$
B_1	1.2 km
B_2	1.0 km
r_f	range to front center, 60 km
L	front width, 20 km
g	0.017
$\eta(r, z)$	$2\{[z - z_0(r)]/B(r)\}$
$z_0(r)$	depth of channel axis, $z_{01} - [(B_2 - B_1)/2] \tanh\{(r - r_f)/L\}$
z_{01}	initial depth of sound channel axis at $r = 0$ km, 0.8 km.

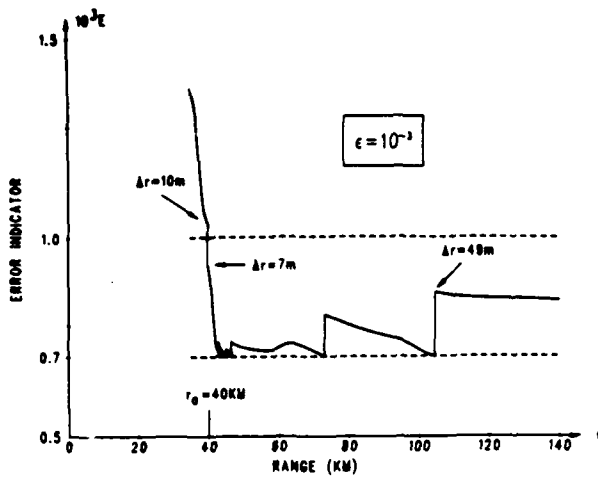


FIG. 10. Error indicator E versus range r for the environment of Fig. 9; $f = 100$ Hz; $h_s = 100$ m; $r_0 = 40$ km; and $\epsilon = 10^{-3}$.

which was used in Ref. 18. At cut-in, the error indicator happens to be just outside the window and the step size drops to $\Delta r = 7$ m. At about $r = 42$ km, the error has fallen enough so that the first step size increase occurs. Then, several step increases in a row occur. Note that the error indicator does not increase significantly in this region. Then, at nearly 50 km, E becomes virtually constant for almost 15 km. Finally, it leaves the window, the step size is increased, and this time the error indicator is near the center of the window. At $r = 105$ km, the step size is increased again to $\Delta r = 49$ km, and the error is seen to remain virtually flat out to the maximum range examined in this example. It would appear that, in this last region, the algorithm has found a nearly optimal step size (about three wavelengths), in the sense that the error is virtually constant and the error is near the center of the tolerance window.

Relative intensity curves for this sound channel are shown in Fig. 11. The solid curve depicts I versus range r for a receiver depth of 300 m computed in N mode, while the

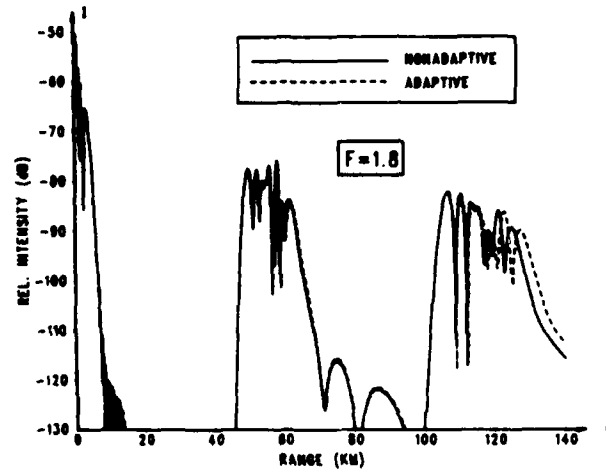


FIG. 11. Relative intensity I versus range r for the deep-ocean channel shown in Fig. 9; $h_r = 300$ m; other parameters as in Fig. 10.

dashed curve represents the intensity for the A mode calculation. The two curves are in excellent agreement throughout the first convergence zone, between about $r = 45$ km to $r = 70$ km, and out through part of the second convergence zone. Beyond about $r = 115$ km, there appears to be some shifting of phase pattern. The A mode curve reflects the qualitative behavior of intensity all the way to $r = 140$ km. For this example, the efficiency factor $F = 1.8$. One reason for the lower value of F is the size of the cut-in range r_0 . While smaller than F values attained for the previous three cases, this still represents a substantial savings of processor time, especially for this computationally intensive example.

IV. SUMMARY

The parabolic approximation to the reduced wave equation has established itself as a formidable propagation model within the underwater acoustics community. Because it includes range-dependent environments, is valid at low frequencies, and can be numerically solved with efficient algorithms, it has become the model of choice for many applications. After very briefly reviewing the origin of the parabolic approximation and related parabolic equations, we summarize pertinent details, such as notation and error characteristics of the widely employed IFD implementation.

We introduce one way to estimate the error from the IFD algorithm. This error only accounts for discretization in range. The error indicator is calculated with an appropriate norm at each step. For a specified error tolerance, a tolerance window is formed by requiring that the error indicator remain below the error tolerance but above 70% of that value. If the error indicator leaves the window, the step size is either increased or decreased. The magnitude of the change is computed from a relationship between step sizes and errors. An additional feature is that the activation of the step changer can be postponed by specifying an additional parameter called the cut-in range. Below this range, no range step changes are made, which may be desirable as the rapid oscillations sometimes present in the start-up field are stripped away. Also, should the ratio of the norm of the solution and the error tolerance drop below a specified value, adaption is terminated. In addition to the standard input and output required by IFD, our enhancements (collectively known as EIFD) require additional input, namely the error tolerance and cut-in range, and generate several additional output files useful for monitoring the error behavior and graphically interpreting the transmission loss or intensity. Because the algorithm controls absolute error, but not relative error, the decibel error in the vicinity of some fades may occasionally be large. Nonetheless, our adaptive enhancements locate these fades and indicate their approximate sizes.

Numerical examples illustrate the performance of our algorithm in a variety of propagation channels. In a shallow isospeed channel, the adaptive algorithm produced nearly a sevenfold improvement (decrease) in run time, due partially to its selection of large step sizes. Two cases of propagation in an isospeed channel with a sloping bottom were examined also. In the first instance, the source was in moderately deep water and the receiver was in very shallow water, while in the

second, the source and receiver were interchanged. Step sizes were found to exhibit interesting changes for propagation either up or down the slope. In the former case, mode cutoff occurred at the top of the slope, eventually leading to the requirement that adaption terminate because solution norm and error tolerance approached comparable magnitudes. In the latter, multiple modes were not excited until well down the slope. It is interesting to note that the adaptive algorithm ran faster for the downslope example. Finally, deep-ocean propagation through a front was studied. Efficiency according to our measure increased by less than a factor of 2, though this represents an enormous savings in computational time.

We have described enhancements to the IFD implementation of the parabolic approximation that can yield significant run-time improvements. An additional approach, which may also offer promise, is to adaptively add (delete) points to (from) the depth mesh grid. An optimal method of simultaneously selecting both range- and depth-mesh increments to minimize solution error is being investigated. These on-going developments suggest additional research directions that can significantly extend the family of underwater acoustic propagation problems that can be solved on current research computers.

ACKNOWLEDGMENT

This work has been supported by Code 11250A, U.S. Office of Naval Research.

¹F. D. Tappert, "The parabolic approximation method," in *Wave Propagation in Underwater Acoustics*, edited by J. B. Keller and J. S. Papadakis (Springer, Berlin, 1977), pp. 224-287.

- ²D. Lee and G. Botseas, "IFD: An implicit finite difference computer model for solving the parabolic equation," New London Lab., NUSC, New London, CT (1982), TR6659, AD-A117 701/3.
- ³H. K. Brock, "The AESD parabolic equation model," NORDA, Bay St. Louis, MS (1978), Tech. Note 12.
- ⁴G. Botseas, D. Lee, and K. E. Gilbert, "IFD: Wide angle capability," New London Lab., New London, CT (1983), TR6905.
- ⁵L. Nghiem-Phu and F. D. Tappert, "A high-speed, compact, and interactive parabolic equation solution generator (PESOGEN)," *J. Acoust. Soc. Am. Suppl.* 1 75, S26 (1984).
- ⁶H. W. Kutschale, "Arctic marine acoustics," Lamont-Doherty Geo. Obs., Columbia University, Palisades, NY (1984), AD-A147 492.
- ⁷J. S. Perkins and R. N. Baer, "An approximation to the three-dimensional parabolic equation method for acoustic propagation," *J. Acoust. Soc. Am.* 72, 515-522 (1982).
- ⁸D. Lee, "The state-of-the-art parabolic equation approximation as applied to underwater acoustic propagation with discussions on intensive computations," NUSC, New London, CT (1984), TD 7247.
- ⁹M. H. Schultz, "Multiple array processors for ocean acoustic problems," *Comput. Math. Appl.* 11, 777-785 (1985).
- ¹⁰J. S. Robertson, W. L. Siegmann, and M. J. Jacobson, "Current and current shear effects in the parabolic approximation for underwater sound channels," *J. Acoust. Soc. Am.* 77, 1768-1780 (1985).
- ¹¹D. Lee and W. L. Siegmann, "Mathematical model for the 3-dimensional ocean sound propagation," *Math. Model.* 7, 143-162 (1986).
- ¹²D. F. St. Mary, D. Lee, and G. Botseas, "A modified wide angle parabolic wave equation," *J. Comp. Phys.* 71, 304-315 (1987).
- ¹³D. Lee and S. T. McDaniel, "Ocean acoustic propagation by finite difference methods," *Comput. Math. Appl.* 14, 305-423 (1987).
- ¹⁴M. Berger and J. Olinger, "Adaptive mesh refinement for hyperbolic partial differential equations," *J. Comput. Phys.* 53, 484-512 (1984).
- ¹⁵D. C. Arney and J. E. Flaherty, "A two-dimensional mesh moving technique for time-dependent partial differential equations," *J. Comput. Phys.* 67, 124-144 (1986).
- ¹⁶D. J. Kewley, L. T. Sin Fai Lam, and G. Gartrell, "Practical solutions of the parabolic equation model for underwater acoustic wave propagation," in *Computational Techniques and Applications: CTAC-83*, edited by J. Noye and C. Fletcher (Elsevier, Amsterdam, 1984), pp. 669-684.
- ¹⁷L. F. Shampine, "The step sizes used by one-step codes for ODEs," *Appl. Num. Math.* 1, 95-106 (1985).
- ¹⁸F. D. Tappert and D. Lee, "A range refraction parabolic equation," *J. Acoust. Soc. Am.* 76, 1797-1803 (1984).

Office of Naval Research
800 North Quincy St.
Arlington, VA 22217-5000
ATT: Code 11250A
Dr. Marshall Orr

Office of Naval Research
Resident Representative
33 Third Avenue - Lower Level
New York, NY 10003-9998

Commanding Officer
Naval Underwater Systems
Center-Newport Laboratory
Newport, RI 02840
ATT: Unclassified Library

Office of Naval Research
800 North Quincy St.
Arlington, VA 22217-5000
ATT: Code 1125
Mr. Marvin Blizzard

Commander
Naval Air Systems Command
Jefferson Plaza #1
1411 Jefferson Davis Hgwy.
Arlington, VA 20360

Superintendent
Naval Postgraduate School
Monterey, CA 93940

Office of Naval Research
800 North Quincy St.
Arlington, VA 22217-5000
ATT: Mr. Robert Peloquin

Commanding Officer
Fleet Numerical Weather
Central
Monterey, CA 93940
ATT: Mr. Paul Stevens

Superintendent
U.S. Naval Academy
Annapolis, MD 21402
ATT: Library

Office of Naval Research
800 North Quincy St.
Arlington, VA 22217-5000
ATT: Code 220

Commander
Naval Ocean Systems Center
Dept. of the Navy
San Diego, CA 92132
ATT: Mr. David Gordon
Code 711

Woods Hole Oceanographic
Institution
Woods Hole, MA 02543
ATT: Dr. James Lynch

Office of Naval Technology
800 North Quincy Street
Arlington, VA 22217-5000
ATT: MAT 0721

Commander
Naval Surface Weapons Center
Acoustics Division
Silver Spring, MD 20910

NORDA
Stennis Space Center
Bay St. Louis, MS 39522
ATT: Dr. W. B. Moseley

Director
Naval Research Laboratory
4555 Overlook Avenue, SW
Washington, D.C. 20375
ATT: Code 2627
(6 copies)

Commander
Naval Air Development Center
Dept. of the Navy
Warminster, PA 18974
ATT: Unclassified Library

NORDA
Stennis Space Center
Bay St. Louis, MS 39522
ATT: Mr. E. Chaika

Director
Office of Naval Research
Branch Office
666 Summer St.
Boston, MA 02210

Commanding Officer
Naval Coastal Systems
Laboratory
Panama City, Florida 32401
ATT: Unclassified Library

Naval Oceanographic Office
Stennis Space Center
Bay St. Louis, MS 39522
ATT: Dr. T. M. Davis

Naval Oceanographic Office
Stennis Space Center
Bay St. Louis, MS 39522
ATT: Dr. W. Jobst

Commanding Officer
Naval Underwater Sys Center
New London, CT 06320
ATT: P. Scully-Power

Commander
David W. Taylor Naval Ship
R & D Center
Bethesda, MD 20084
ATT: Dr. M. Sevik

Chief of Naval Operations
Naval Oceanographic Div.
Department of the Navy
Washington, D.C. 20352
ATT: OP-952

Commanding Officer
Naval Underwater Sys Center
New London, Ct 06320
ATT: Dr. Ding Lee

Marine Physical Laboratory
Scripps Inst. of Oceanog.
U. of California, San Diego
San Diego, CA 92152
ATT: Dr. Daniel Andrews

Commander
SPAWARS
National Center #1
Arlington, VA 20360
ATT: PME 124

Naval Postgraduate School
Monterey, CA 93940
ATT: Dr. C.-S Chiu

Atlantic Oceanographic and
Meteorological Labs
15 Rickenbacker Causeway
Miami, FL 33249
ATT: Dr. John Proni

Commander
Naval Sea Systems Command
National Center #2
Arlington, VA 20362
ATT: SEA 63R

Applied Physics Laboratory
Univ. of Washington
1013 North East 40th Street
Seattle, Washington 98105
ATT: Dr. T. E. Ewart

University of Michigan
Cooley Electronics
Laboratory
Ann Arbor, MI 48105
ATT: Dr. T. G. Birdsall

Defense Documentation Center
Cameron Station, Bldg. 5
Alexandria, VA 22314
(12 copies)

Scripps Inst. of Oceanography
Univ. of California
La Jolla, CA 92093
ATT: Dr. W. Munk

University of Rhode Island
Dept. of Oceanography
Wakefield, RI 02881

Commanding Officer
Naval Underwater System Center
New London, CT 06320
ATT: Dr. William Von Winkle

University of Miami
4600 Rickenbacker Causeway
Miami, FL 33149
ATT: Dr. H. DeFerrari

Office of the Assistant
Secretary of the Navy
RM 5E779 Pentagon
Washington, D.C. 20350
ATT: Dr. J. H. Probus

Commanding Officer
Naval Underwater Systems Center
New London, CT 06320
ATT: Dr. D. M. Viccione

Chief of Naval Operations
Room 5D580, Pentagon
Washington, D.C. 20350
ATT: OP951F

Commander
Naval Sea Systems Command
Washington, D.C. 20362
ATT: PMS 409

Defense Advanced Research
Projects Agency
1400 Wilson Blvd.
Arlington, VA 22209

Commander
Naval Surface Weapons Center
Dahlgren, VA 22448
ATT: Dr. E. W. Schwiderski
Code K05

Applied Physics Laboratory
Univ. of Washington
1013 North East 49th Street
Seattle, Washington 98105

END OF LIST 1
(61 copies)

NORDA
Stennis Space Center
Bay St. Louis, MS 39522
ATT: Mr. R. Van Wyckhouse

Commander
Oceanographic System
Atlantic
Box 100
Norfolk, VA 23511

Chase, Inc.
14 Pinckney St.
Boston, MA 02114
ATT: Dr. David Chase

Naval Oceanographic Office
Stennis Space Center
Bay St. Louis, MS 39522
ATT: Mr. W. H. Geddes

Commander
Oceanographic System
Pacific
Box 1390
Pearl Harbor, Hawaii 96860

Dr. David Middleton
127 East 91st Street
New York, NY 10028

Naval Oceanographic Office
Stennis Space Center
Bay St. Louis, MS 39522
ATT: Mr. R. Merrifield

Commanding Officer
Fleet Weather Central
Box 113
Pearl Harbor, Hawaii 96860

Duke University
Dept. of Electrical Eng.
Durham, NC 27706
ATT: Dr. Loren Nolte

Naval Oceanographic Office
Stennis Space Center
Bay St. Louis, MS 39522
ATT: M. K. Shank

Naval Ocean Systems Center
(Kaneohe)
Kaneohe, Hawaii 96863
ATT: Mr. D. Hightower

Gould, Incorporated
Chesapeake Instrument Div.
6711 Baymeadow Drive
Glen Burnie, MD 21061
ATT: Dr. O. Lindemann

Superintendent
Naval Research Laboratory
Underwater Sound Ref. Div.
P. O. Box 8337
Orlando, Florida 32806

Commander
Naval Ocean Systems Center
Dept. of the Navy
San Diego, CA 92132
ATT: Mr. Ted Wright
Code 541

G. R. Associates, Inc.
10 Columbia Corporate Center
10400 Little Patuxent Pk'way
Suite 430
Columbia, MD 21044

Director
Office of Naval Research
Branch Office
1030 East Green Street
Pasadena, CA 91106

Commanding Officer
Naval Intelligence Support
Center
4301 Suitland Road
Washington, DC 20390
ATT: NISC 20

Hughes Aircraft Company
P. O. Box 3310
Fullerton, CA 92634
ATT: Mr. S. W. Autrey

Director
Office of Naval Research
Branch Office
536 South Clark St.
Chicago, Illinois 60605

Bolt, Beranek, & Newman, Inc.
50 Moulton Street
Cambridge, MA 02238
ATT: Dr. K. L. Chandiramani

University of Michigan
Dept. of Aerospace Eng.
North Campus
Ann Arbor, MI 48109
ATT: Dr. W. W. Wilmarth

REPORT DOCUMENTATION PAGE		READ INSTRUCTIONS BEFORE COMPLETING FORM
1. REPORT NUMBER RPI Math. Rep. No. 177	2. GOVT ACCESSION NO.	3. RECIPIENT'S CATALOG NUMBER
4. TITLE (and Subtitle) An Efficient Enhancement of Finite-Difference Implementations for Solving Parabolic Equations		5. TYPE OF REPORT & PERIOD COVERED
		6. PERFORMING ORG. REPORT NUMBER
7. AUTHOR(s) J. S. Robertson, M. J. Jacobson, W. L. Siegmann, and D. C. Arney		8. CONTRACT OR GRANT NUMBER(s) N00014-86-K-0129
9. PERFORMING ORGANIZATION NAME AND ADDRESS Rensselaer Polytechnic Institute Troy, New York 12180-3590		10. PROGRAM ELEMENT, PROJECT, TASK AREA & WORK UNIT NUMBERS NR 4254007
11. CONTROLLING OFFICE NAME AND ADDRESS Office of Naval Research, Code 1125 OA Department of the Navy Arlington, Virginia 22217-5000		12. REPORT DATE September 15, 1989
		13. NUMBER OF PAGES 14
14. MONITORING AGENCY NAME & ADDRESS (if different from Controlling Office)		15. SECURITY CLASS. (of this report)
		15a. DECLASSIFICATION/DOWNGRADING SCHEDULE
16. DISTRIBUTION STATEMENT (of this Report) This document has been approved for public release and sale; its distribution is unlimited.		
17. DISTRIBUTION STATEMENT (of the abstract entered in Block 20, if different from Report)		
18. SUPPLEMENTARY NOTES		
19. KEY WORDS (Continue on reverse side if necessary and identify by block number) Ocean Acoustics Parabolic Approximation Finite-Difference Implementations Adaptive Methods		
20. ABSTRACT (Continue on reverse side if necessary and identify by block number) The parabolic approximation method is widely recognized as useful for accurately analyzing and predicting sound transmission intensity in diverse ocean environments. One reason for its attractiveness is that solutions are marched in range, thereby avoiding the large internal storage requirements when using the full wave equation. Present finite-difference implementations employ a range step size that is prescribed (continued on back)		

by either the user or the code and that remains fixed for the duration of the computation. An algorithm is presented in which the range step adaptively selected by a procedure within a version of the implicit finite-difference(IFD) implementation of the parabolic approximation. An error indicator is computed at each range step, and its value is compared to an error tolerance window that is readily specified by the user. If the error indicator falls outside this window, a new range step size is computed and used until the error indicator again leaves the tolerance window. Furthermore, for a given tolerance, this algorithm generates a range step size that is optimal in a specified sense and that often leads to large decreases in run time. Additional related modifications to the IFD implementations are discussed. Several examples are presented that illustrate the efficacy of the enhanced algorithm.